Supplementary Information

Tailoring thermal expansion and luminescence thermometric performance of $KMgScW_3O_{12}$-based compounds

Ming Li [1], Qi Miao[1], Kaiyue Zhao[1], Yangke Cun*[2], Yongqiang Qiao[1], Juan Guo[1], Li Li*[3] and Qilong Gao*[1]

1 School of Physics and Microelectronics, Zhengzhou University, Zhengzhou, 450001, China

2College of Materials Science and Engineering, Kunming University of Science and Technology, Kunming 650093, China

3College of Science, Chongqing University of Posts and Telecommunications, Chongqing400065, P. R. China

*E-mail: cunyangke@126.com; lilic@cqupt.edu.cn; qilonggao@zzu.edu.cn

1. Experiment and data analysis details

Materials Synthesis. We used the high-temperature solid-state method to synthesize $(KMg)_xSc_{1.82-x}W_3O_{12}$: 0.15Yb/0.03Er samples, which were not pure when $x < 0.4$. The raw materials are K_2CO_3 (99%, Macklin), MgO (99%, Macklin), Sc_2O_3 (99.99%, Macklin), WO_3 (99%, Macklin), Yb_2O_3 (99.99%, Macklin), Er_2O_3 (99.99%, Macklin). The raw material mixture was ground in a mortar for 2 h according to the molar ratio, and then the powder sample was poured into a Pt crucible, sintered in a Muffle furnace at 873 K for 6 h, and then cooled to room temperature (RT) naturally. The obtained sample was ground again for 2 h and pressed into cylindrical pellets with a diameter of 8 mm, and sintered at a high temperature of 1223 K for 24 h to obtain a pure target product.

Sample Characterizations. XRD was measured with Cu Kα using the Rigaku diffractometer (Japan, Smart Lab 3 KW, λ = 1.5406 Å). Variable-temperature XRD diffraction data were collected at 0.01° steps in the 2θ range of 10-120°. The crystal structure of the sample was mapped by VESTA software. Temperature-dependent Raman spectrum (wavelength of excitation 633 nm, RT-700 K) was recorded using a Raman spectrometer (France, HORIBA, Lab RAM HR Evolution). The surface morphology was measured using field emission scanning electron microscopy (SEM, Zeiss/Auriga FIB). FEI Talos F200S was used to observe the element distribution of the sample by high-resolution transmission electron microscopy (HRTEM). X-ray

photoelectron spectroscopy (XPS) data were acquired with Al Kα radiation (Escalab 250Xi) and corrected with C 1s spectral lines (284.8 eV). The thermal stability of the sample was tested by a Mettler DSC3 differential scanning calorimeter at a temperature rise rate of 10 K/min. A spectrophotometer (Carry 5000 UV-Vis-NIR, America) was used to record the UV/Vis spectra. The temperature-dependent photoluminescence emission spectrum and decay curve were measured using the Edinburgh FLS1000 steady-state fluorescence spectrometer connected to a temperature controller (HFS600E-PB2)

Computational methods. All calculations were performed using first principles method based on density functional theory (DFT) as implemented in the Vienna *ab initio* simulation package (VASP) .[1] The projector augmented wave (PAW) method was used to describe the ion-electron interaction.[2] The generalized gradient approximation (GGA) function of Perdew, Burke, and Ernzerhof (PBE) was used to describe the exchange and correlation effects. A plane-wave energy cutoff of 550 eV was used here,[3] with a 6 × 6 × 6 Monkhorst-Pack *k*-point mesh to sample the Brillouin zone. The convergence values were set to 10^{-8} eV/atom for the calculation of the total energy, to 10^{-4} eV/atom for the residual forces during the structure relaxation.[4]

2. Supplementary Figures and Tables

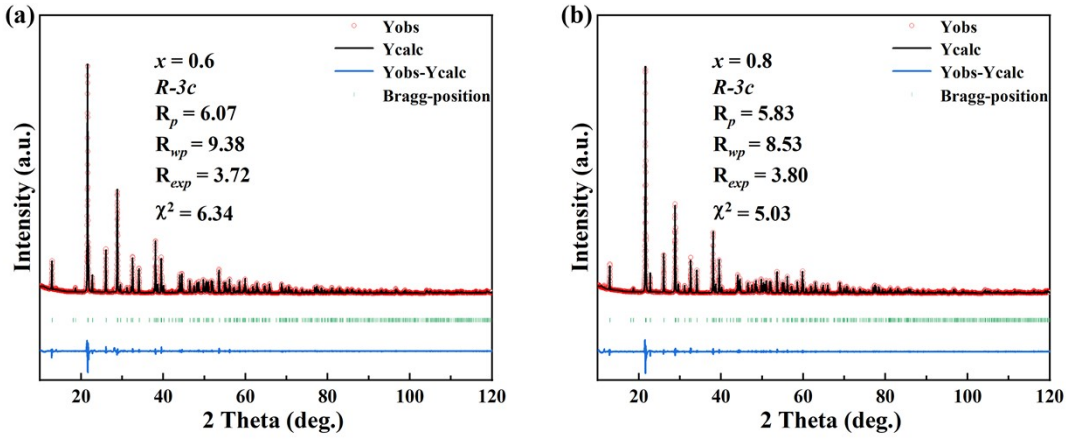

Fig.S1. Rietveld refinement results of XRD pattern at RT of (a) KM6 sample and (b) KM8 sample.

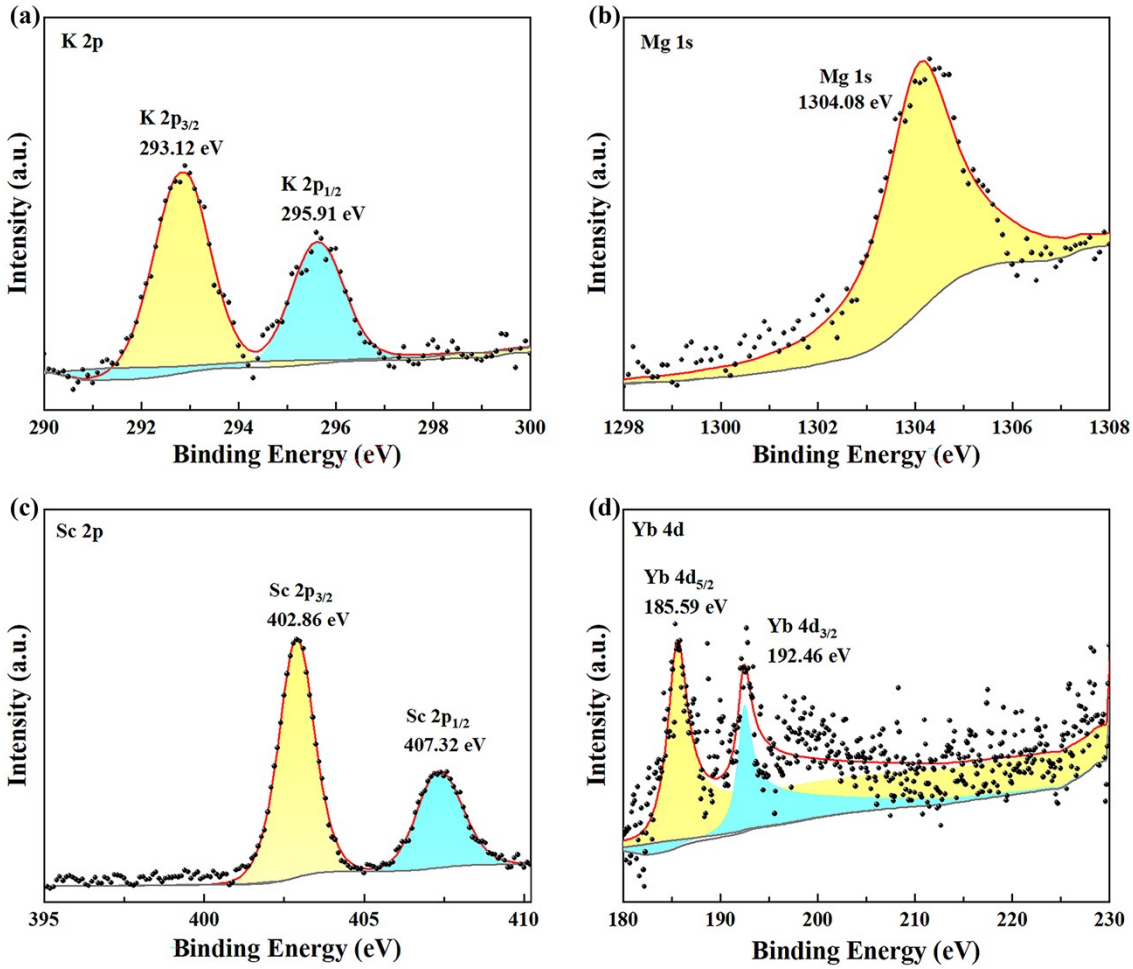

Fig.S2. XPS spectra of KM4 sample. (a) K 2p peaks. (b) Mg 1s peak. (c) Sc 2p peaks. (d) Yb 4d peaks.

The two peaks observed in the K 2p XPS spectra of the sample at 295.91 eV and 293.12 eV belong to K $2p_{1/2}$ and K $2p_{3/2}$, respectively, indicating the presence of K element in the sample as a +1 valence state. The Mg 1s peak is located at 1304.08 eV, indicating that the valence state of Mg is +2. Sc 2p also splits into two peaks with binding energies of 407.32 eV and 402.86 eV respectively, belonging to Sc $2p_{1/2}$ and Sc $2p_{3/2}$, indicating that Sc is in a +3 valence state. Yb 4d also observed two peaks at 192.46 eV and 185.59 eV, belonging to Yb $4d_{1/2}$ and Yb $4d_{5/2}$, respectively, indicating that Yb exists in the sample as a +3 valence state.

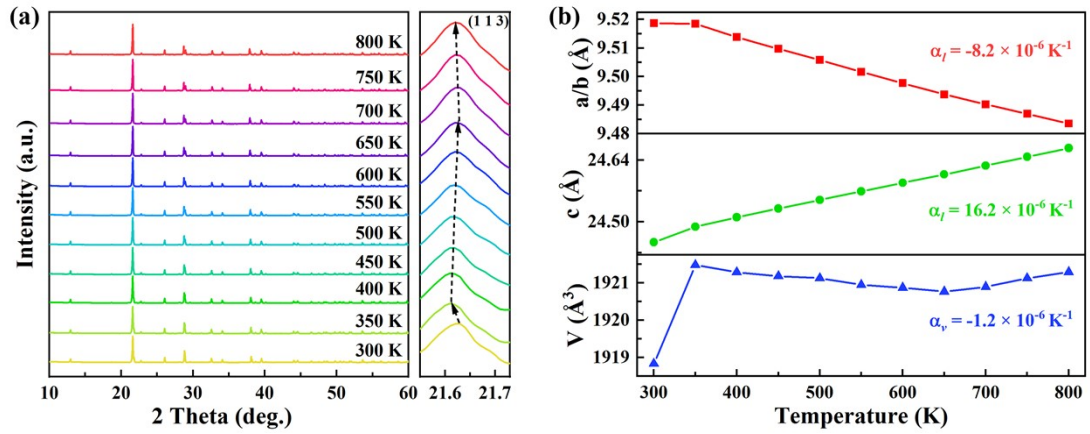

Fig.S3. (a) Temperature-dependent XRD patterns and local amplification of KM6 sample (300-800 K). (b) Temperature dependence of lattice parameters and unit cell volume of KM6 sample.

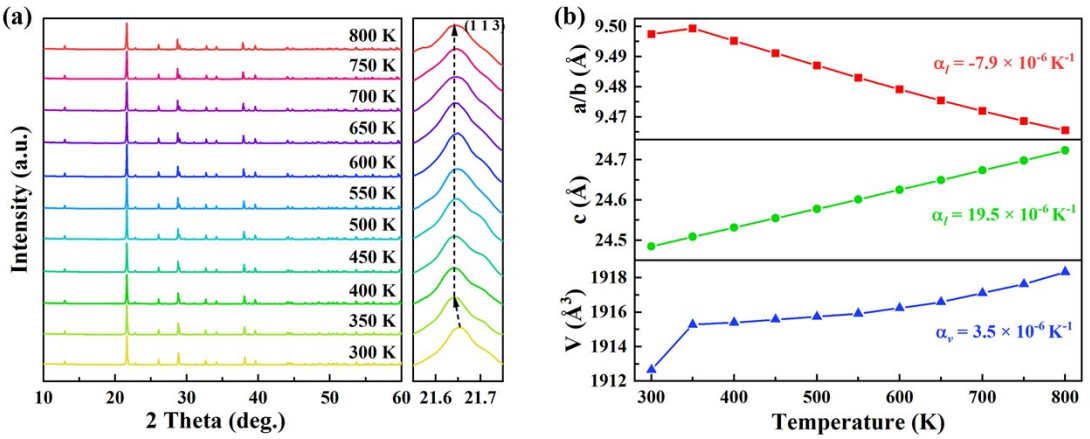

Fig.S4. (a) Temperature-dependent XRD patterns and local amplification of KM8 sample (300-800 K). (b) Temperature dependence of lattice parameters and unit cell volume of KM8 sample.

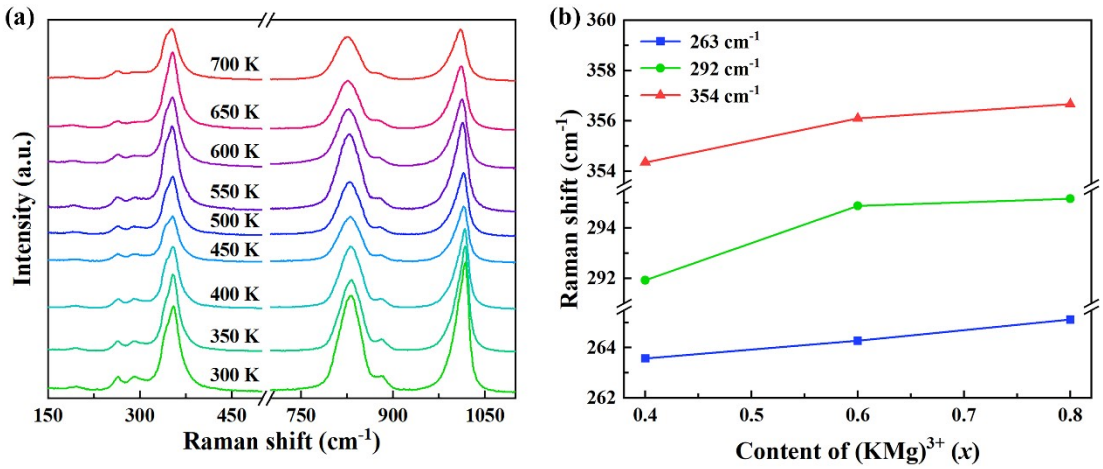

Fig.S5. (a) Raman spectra of KM4 at different temperatures. (b) The frequency shifts of Raman modes corresponding to KM4, KM6 and KM8 samples change with $(KMg)^{3+}$

ions at RT.

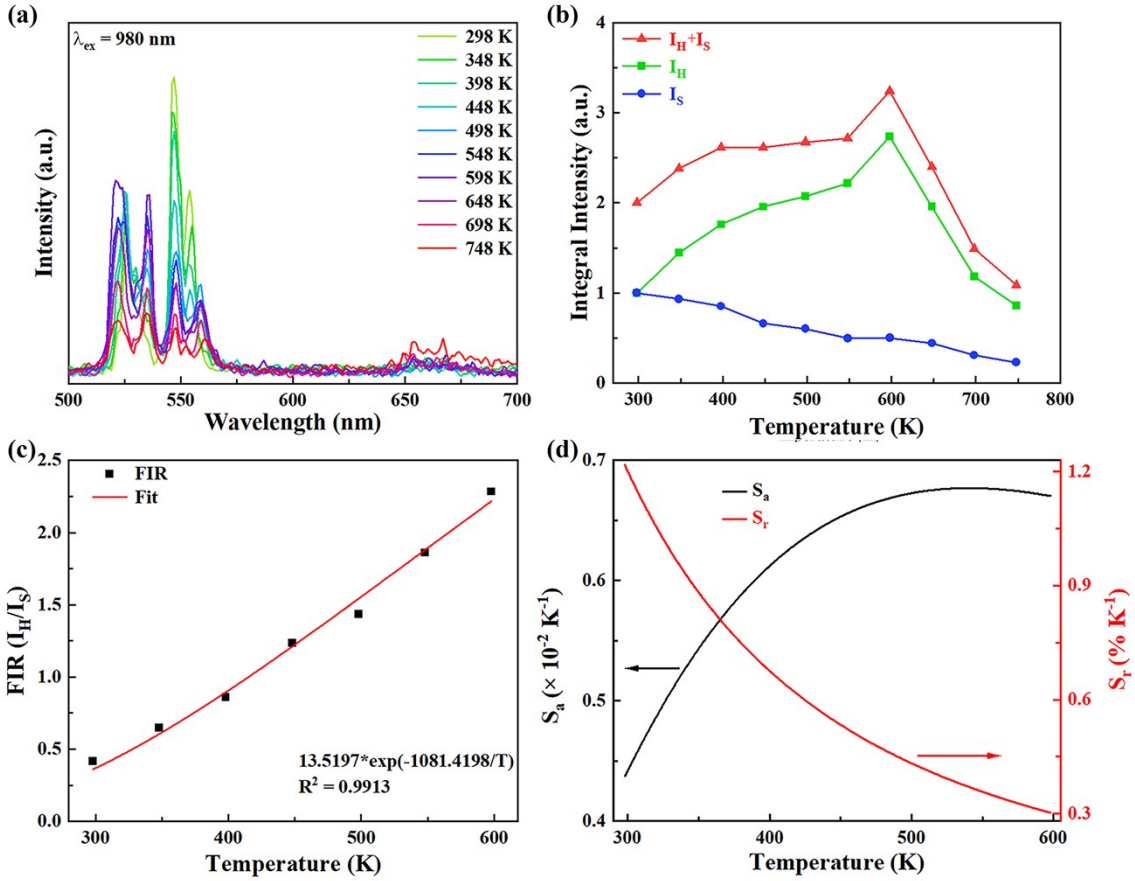

Fig.S6. (a) UCL emission spectra of KM6 sample at 298-748 K under 980 nm laser excitation. (b) The corresponding UCL emission integral intensities of $^2H_{11/2(2)}/^2H_{11/2(1)}$, $^4S_{3/2(2)}/^4S_{3/2(1)}$ and total ($^2H_{11/2}$ + $^4S_{3/2}$) levels of Er^{3+} ions. (c) The relationships between FIR values and sample temperature. (d) The absolute sensitivity S_a and relative sensitivity S_r curves.

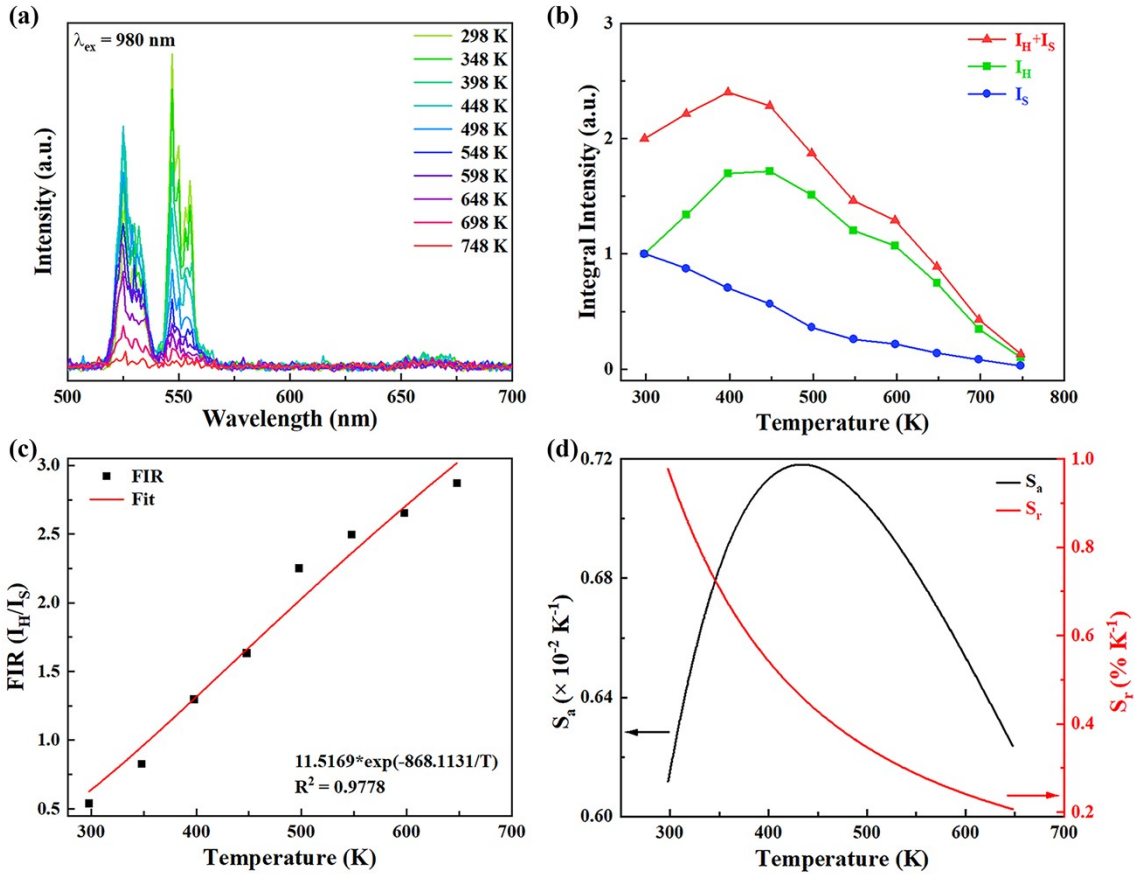

Fig.S7. (a) UCL emission spectra of KM8 sample at 298-748 K under 980 nm laser excitation. (b) The corresponding UCL emission integral intensities of $^2H_{11/2(2)}/^2H_{11/2(1)}$, $^4S_{3/2(2)}/^4S_{3/2(1)}$ and total ($^2H_{11/2} + ^4S_{3/2}$) levels of Er^{3+} ions. (c) The relationships between FIR values and sample temperature. (d) The absolute sensitivity S_a and relative sensitivity S_r curves.

Table S1. The lattice parameters obtained by the XRD refinement of KM4 sample.

Temperature	Lattice parameters		
(K)	*a*/*b* (Å)	*c* (Å)	*V* (Å^3)
300	9.53897 (8)	24.41263 (23)	1923.748 (29)
350	9.53780 (8)	24.46324 (23)	1927.262 (29)
400	9.53271 (8)	24.48368 (25)	1926.813 (30)
450	9.52867 (8)	24.49965 (25)	1926.439 (30)
500	9.52483 (8)	24.51474 (25)	1926.073 (31)
550	9.52089 (8)	24.52910 (25)	1925.607 (31)
600	9.51726 (9)	24.54392 (26)	1925.301 (32)
650	9.51367 (9)	24.55885 (27)	1925.019 (34)
700	9.51005 (9)	24.57264 (28)	1924.632 (35)
750	9.50683 (10)	24.58739 (29)	1924.487 (36)
800	9.50365 (10)	24.60163 (31)	1924.312 (38)

Table S2. The structural parameters obtained by the XRD refinement of KM4 sample at 300 K.

Atom	*x*	*y*	*z*	*Occ.*
K (6b)	0.00000	0.00000	0.00000	0.400
Sc5/Mg4 (12c)	0.00000	0.00000	0.13978	1.600/0.400
W3 (18e)	0.28116	0.00000	0.25000	3.000
O1 (36f)	0.04890	0.19210	0.18520	6.000
O2 (36f)	0.17340	0.13380	0.09720	6.000
Yb (12c)	0.00000	0.00000	0.13978	1.600/0.400
Er (12c)	0.00000	0.00000	0.13978	1.600/0.400
a/b (Å)			9.538970	
c (Å)			24.412630	
V (Å^3)			1923.748 (29)	
R_p (%)			5.77	
R_{exp} (%)			3.65	

Table S3. The structural parameters obtained by the XRD refinement of KM4 sample at 800 K.

Atom	*x*	*y*	*z*	*Occ.*
K (6b)	0.00000	0.00000	0.00000	0.400
Sc5/Mg4 (12c)	0.00000	0.00000	0.14210	1.600/0.400
W3 (18e)	0.28116	0.00000	0.25000	3.000
O1 (36f)	0.05560	0.19920	0.18940	6.000
O2 (36f)	0.18350	0.13880	0.09470	6.000
Yb (12c)	0.00000	0.00000	0.14210	1.600/0.400
Er (12c)	0.00000	0.00000	0.14210	1.600/0.400
a/b (Å)			9.503650	
c (Å)			24.601633	
V (Å^3)			1924.312 (38)	
R_p (%)			5.50	
R_{exp} (%)			3.68	

Table S4. The bond angles obtained by the XRD refinement of KM4 sample.

Temperature	Bond angles (°)	
(K)	Sc5–O1–W3	Sc5–O2–W3
300	147.0 (4)	152.3 (6)
350	146.8 (4)	151.6 (6)
400	146.7 (4)	150.2 (6)
450	146.5 (4)	149.7 (6)
500	146.1 (4)	149.4 (6)
550	145.8 (4)	149.0 (6)
600	145.7 (5)	148.1 (6)
650	144.9 (5)	147.8 (6)
700	144.4 (5)	146.7 (6)
750	144.4 (5)	147.0 (6)
800	143.2 (5)	145.8 (6)

Table S5. The interatomic distance of between the closest identical atoms obtained by the XRD refinement of KM4 sample.

Temperature	Interatomic distance (Å)	
(K)	Sc5–Sc5	W3–W3
300	5.6630 (2)	4.9487 (3)
350	5.6570 (2)	4.9560 (3)
400	5.6516 (19)	4.9585 (3)
450	5.6478 (19)	4.9599 (3)
500	5.6450 (2)	4.9610 (3)
550	5.6400 (2)	4.9624 (3)
600	5.6380 (2)	4.9639 (3)
650	5.6330 (2)	4.9652 (3)
700	5.6300 (2)	4.9666 (3)
750	5.6250 (2)	4.9679 (3)
800	5.6200 (2)	4.9692 (3)

Table S6. The total anharmonicity has been determined from the temperature-dependency of the Raman frequencies shown in Figure 4(d).

Mode frequency ω_i (cm^{-1})	$(\frac{\partial \omega_i}{\partial T})_P$ ($cm^{-1}\,K^{-1}$)	Total anharmonicity ($\times 10^{-5}\,K^{-1}$)
264.0	-0.00169	-0.64
291.9	0.00313	1.07
340.6	0.00373	1.10
354.3	-0.00262	-0.74
831.1	-0.01358	-1.63
885.4	-0.01228	-1.39
1014.5	-0.01693	-0.17

Table S7. Temperature sensing performance of rare earth ions activated luminescent material thermometer.

Materials	Temperature range (K)	$S_a$max ($\times 10^{-2}$ K^{-1})	$S_r$max (% K^{-1})	Ref.
$Gd_{9.33}(SiO_4)_6O_2$: Yb^{3+}/Er^{3+}	298-548	0.46	-	5
$NaLuF_4$: Eu^{3+}@g-C_3N_4	303-503	0.57	0.46	6
BaY_2O_4: Er^{3+}/Yb^{3+}	298-573	0.19	-	7
$Ca_8ZnLa(PO_4)_7$: Tb^{3+}/Eu^{3+}	298-448	-	0.53	8
$Na_{0.5}Bi_{0.5}TiO_3$: Er^{3+}	93-553	0.35	-	9
$Zn_3Mo_2O_9$: Er^{3+}	373-573	0.60	0.72	10
$(KMg)_{0.4}Sc_{1.42}W_3O_{12}$: 0.15Yb/0.03Er	298-748	0.50	0.86	This work

References

1 L. H. N. Rimmer, M. T. Dove, A. L. Goodwin and D. C. Palmer, *Phys. Chem. Chem. Phys.*, 2014, **16**, 21144-21152.

2 G. Kresse and D. Joubert, *Phys. Rev. B*, 1999, **59**, 1758-1775.

3 Z. Wang, F. Wang, L. Wang, Y. Jia and Q. Sun, *J. Appl. Phys.*, 2013, **114**.

4 M. K. Gupta, B. Singh, R. Mittal, S. Rols and S. L. Chaplot, *Phys. Rev. B*, 2016, **93**.

5 J. Zhang and F. Qian, *Dalton T.*, 2020, **49**, 10949-10957.

6 P. Du, J. Tang, W. Li and L. Luo, *Chem. Eng. J*, 2021, **406**, 127165.

7 G. Xiang, X. Liu, Q. Xia, S. Jiang, X. Zhou, L. Li, Y. Jin, L. Ma, X. Wang and J. Zhang, *Inorg. Chem.*, 2020, **59**, 11054-11060.

8 L. Li, X. Tang, Z. Wu, Y. Zheng, S. Jiang, X. Tang, G. Xiang and X. Zhou, *J. Alloys Compd.* , 2019, **780**, 266-275.

9 P. Du and J. S. Yu, *Ceram. Int.*, 2015, **41**, 6710-6714.

10 H. Liu, H. Wang, X. Zheng, P. Wang and Y. Zhang, *Dalton T.*, 2022, **51**, 13106-13118.